

Combined remoderation-drift scheme for positron injection into a magnetic trapU. Hergenhahn ^{1,2} J. Horn-Stanja,¹ S. Nißl ^{1,3} H. Saitoh ^{1,4} M. Singer ^{1,3} T. Sunn Pedersen,^{1,5,*} C. Hugenschmidt ³ and E. V. Stenson ^{1,†}¹Max Planck Institute for Plasma Physics, 85748 Garching and 17491 Greifswald, Germany²Fritz-Haber-Institut der Max-Planck-Gesellschaft, 14195 Berlin, Germany³Technische Universität München, 85748 Garching, Germany⁴Graduate School of Frontier Sciences, The University of Tokyo, Kashiwa, Chiba 277-8561, Japan⁵Institute of Physics, The University of Greifswald, 17489 Greifswald, Germany

(Received 21 October 2022; accepted 23 May 2023; published 20 June 2023)

The efficient transfer of a magnetically guided positron beam into a region of closed magnetic field lines is nontrivial. An $\mathbf{E} \times \mathbf{B}$ -drift technique has previously been used effectively to inject a low-energy (5- to 20-eV) positron beam into the confinement region of a permanent-magnet-based dipole trap. To complement and extend that strategy, we have investigated an approach in which a high-energy (~ 350 -eV) positron beam is remoderated in a SiC crystal immediately outside the confinement region; the reemitted low-energy positrons are then drift injected. Thus we effectively combine positron remoderation and $\mathbf{E} \times \mathbf{B}$ -drift injection in the same spatial region. Initial tests with this scheme were shown to have an overall efficiency of up to $15(\pm 1)\%$. Positron trajectory simulations enabled us to account for various loss mechanisms and thereby identify means to improve this in future implementations. This method adds further flexibility to the search for an efficient injection scheme into toroidal magnetic traps with the mission of confining electron-positron pair plasmas.

DOI: [10.1103/PhysRevResearch.5.023172](https://doi.org/10.1103/PhysRevResearch.5.023172)**I. INTRODUCTION**

Traps for charged particles are used in a great variety of scientific experiments, with goals ranging from precise measurements of fundamental physical constants [1,2], to the generation of antihydrogen atoms and molecules [3,4], to energy production via nuclear fusion [5]. One among these is the goal of creating and studying “pair plasma” composed of equal amounts of electrons and positrons; due to its unique mass symmetry, it has been predicted to behave substantially differently in certain noteworthy ways from electron-ion plasma [6]. A magnetic dipole field produced by a levitated, superconducting current loop has been identified as an attractive confinement scheme for a low-temperature, low-density electron-positron plasma [7]; a second promising option is the twisted, toroidal magnetic field of a stellarator [7].

Filling a magnetic trap with charged particles from an external source is challenging, as the same physics that confines particles inside the trap prevents the passage of external particles from free onto trapped orbits. Nevertheless, our collaboration has previously demonstrated efficient injection of

positrons into the confinement region of a prototype dipole trap based on a supported permanent magnet [8,9]. These experiments used a localized electric field designed to generate an $\mathbf{E} \times \mathbf{B}$ drift that pushes particles from “open” field lines (connecting back to the positron source) to “closed” ones (folding onto themselves, thereby connecting only to the magnet). This results in transient trapping, which can then be extended by five orders of magnitude (from ~ 10 μ s to > 1 s) by switching off the electric field after injection [10]. This scheme has been applied successfully to small populations of “slow” positrons (with kinetic energies of 20 eV and lower) being injected into regions with intermediate magnetic field strength (typically in the tens of mT). Extending injection techniques to higher-field magnetic trapping regions and to a greater variety of velocity and spatial distributions of incoming particles are essential next steps on the way to pair plasma confinement.

Here, we will demonstrate that high-energy positrons can be injected into a prototype dipole magnetic field by inelastic scattering (“reflection remoderation”) on a SiC surface adjacent to the dipole region, followed by $\mathbf{E} \times \mathbf{B}$ -drift injection over a small distance. The latter is essentially similar to the approach used successfully earlier with positrons remoderated outside of the trap [9]. However, the remoderation near to the trap is potentially a useful tool for accumulating low-energy positrons in toroidal field confinement configurations, such as levitated dipoles or stellarators. Probably the most important benefit is that this solves a challenge related to conservation of the first adiabatic invariant $\mu = mv_{\perp}^2/2B$ (the magnetic moment) [11] when injecting into magnetic traps with strong magnetic field strengths. Here, m denotes the electron mass,

*Present address: Type One Energy Group, Madison, WI 53703, USA.

†eve.stenson@ipp.mpg.de

Published by the American Physical Society under the terms of the [Creative Commons Attribution 4.0 International](https://creativecommons.org/licenses/by/4.0/) license. Further distribution of this work must maintain attribution to the author(s) and the published article’s title, journal citation, and DOI. Open access publication funded by the Max Planck Society.

v_{\perp} the velocity component perpendicular to the direction of the magnetic field, and B the magnetic flux density. In the following we will first expand on the concept of μ conservation and after that give some background on positron (re)moderation.

In a future pair plasma trap, a strong magnetic field will be highly advantageous, even necessary, in order to maximize confinement and to make cyclotron cooling effective. It had been predicted, for example, that a magnetic field strength above 2 T would allow the particle confinement time to exceed the cyclotron cooling time even in a simple, four-coil stellarator (i.e., without optimization of the magnetic field for the confinement of single-particle drifts) [12]. The confinement region of the levitated dipole trap currently under construction in our group is planned to have a magnetic field ranging from 14 to 380 mT on the outer midplane (0.65–1.4 T on the inner midplane). When injecting charged particles from weaker into much stronger magnetic fields, however, conservation of the first adiabatic invariant can hinder the injection process via the well known magnetic mirroring mechanism [11]. Thus, μ conservation imposes a strict limit on what strength of magnetic field a given particle can reach. The efficiency with which a collection—i.e., a beam or pulse—of magnetically guided charged particles can be injected into a region of increased magnetic flux density is determined by the ensemble's starting magnetic field and velocity distribution. Preacceleration of charged particles (launching them with a larger v_{\parallel} for a given v_{\perp} distribution) can enable them to reach higher-field regions, but this excess energy is undesirable for applications where low temperatures are needed. In the case of pair plasma creation, e.g., higher incoming particle velocities are likely to produce a higher-temperature electron-positron cloud and correspondingly a longer characteristic shielding distance; this makes it more challenging to get to the small-Debye-length regime where electrostatic collective effects come into play [12,13].

To avoid these problems, minimization of the initial perpendicular temperature is desirable. The standard approach to accumulating, cooling, and tailoring the properties of a beam of positrons is a “buffer-gas trap” [14,15]; in this device, background gases are deliberately introduced that have electronic and vibrational transitions with suitable energies and cross sections for a large fraction (e.g., 10–20%) of the incoming positrons to lose energy without annihilating. Another approach is to cool the positrons' perpendicular temperature via emission of cyclotron radiation in a strong-field linear magnetic trap [15,16]. A third alternative for cooling positrons involves having them interact with one or more lower-temperature plasmas/charged particle clouds [17,18]. The first two of these strategies are, in fact, planned for inclusion in the positron accumulation section of the final pair plasma set-up [7]. However, the tens to hundreds of volts employed for confining large numbers of positrons in such traps have the potential to result in higher parallel energies of the released pulses than are desirable for the pair plasma. One possible solution to these conflicting requirements is the addition of a remoderation stage.

“(Re)moderation” is the process by which energetic positrons impinging on a solid are thermalized by a succession of inelastic collisions. Some of them are then reemitted at a

small kinetic energy, corresponding to the negative sign of the positron work function of the solid. This technique is used to enhance beam brightness at the expense of intensity; the moderation efficiency is strongly dependent on both the remoderator and the energy of the incoming beam, as described in recent reviews [15,19]. Remoderation has the potential to solve previously mentioned difficulties related to μ conservation and/or unwanted kinetic energy: positrons that had been accelerated to higher parallel velocities to reach the strong-field region can there be remoderated down to the lower kinetic energies that are desired. The injection of positrons into a high-field magnetic trap and subsequent remoderation in a metal surface has indeed already been demonstrated; this was performed in a linear trap geometry and combined with energy loss in a high-density electron plasma and an ion cloud [17]. 4H-SiC single crystals are another promising candidate for remoderation, now using a reflection geometry (in which remoderated positrons are emitted from the same face of the remoderator on which they were implanted). The properties of SiC as an alternative to metal foils or crystals have been studied for some time [20], and a further increase in remoderation efficiency was reported for an SiC crystal terminated by an epitaxially grown, nitrogen doped SiC layer [21].

Both our previous experiments and the ones we will describe here were carried out at the reactor-based positron beam line NEPOMUC [22], hosted by the neutron source FRM II (Munich, Germany). This facility produces an intense positron beam (“primary beam”), the energy of which is electrostatically controlled, with a usual value of 1 keV and an intensity of up to $>1 \times 10^9$ positrons per second. In the standard setup for experiments, positrons are then remoderated with a tungsten single crystal in reflection geometry [23], prior to being magnetically guided down the 5-mT NEPOMUC beam line to the experiment stations. The NEPOMUC beam remoderated in this way can reach $>5 \times 10^7$ positrons per second [24]. We have also recently demonstrated the production of the primary beam at significantly lower energies, followed by transport and drift injection into our prototype dipole trap. Despite having a larger spatial spread than the remoderated beam and lower intensity than the 1-keV primary beam, the 20-eV primary beam generated a record rate of $8 \times 10^7 e^+/s$ injected into the dipole [25]. The velocity distribution of the incoming positrons and the transiently trapped orbits in the trap onto which they were injected were similar to those studied previously [9].

In this paper, we report on a complementary approach in which high-energy positrons from the NEPOMUC primary beam were transported to the trap, remoderated on a SiC surface just outside the confinement region, then immediately $\mathbf{E} \times \mathbf{B}$ -drift injected into the trap. Essentially, we “relocated” the remoderation step from being tens of meters upstream (at the NEPOMUC remoderator) to being within centimeters of the trapping region; we will refer to this as “*in situ* remoderation”. Whereas the NEPOMUC remoderator is purposefully placed in a region of minimal magnetic field [24], the SiC crystal for these experiments was located in 15–25 mT (3–5 times stronger than the NEPOMUC guide field). In future devices, it could be located in significantly higher-field regions.

There are also other advantages of *in situ* moderation that can be incorporated into injection schemes. Because

remoderated positrons have a lower kinetic energy, they can be trapped by electrostatic potential barriers that the original, higher-energy beam was—or would have been—able to penetrate. Additionally, high-energy positrons can pass through regions of electric field orthogonal to their direction of travel with negligible deflection, whereas the perpendicular deflection is much greater for low-energy (remoderated) positrons traveling back through the same region. This is the case not only for electrostatic deflection but also for magnetically guided positrons, whose perpendicular $\mathbf{E} \times \mathbf{B}$ -drift velocity is independent of particle kinetic energy. The injection technique we describe here takes advantage of both of these effects. In the following sections, we explain the test geometry in detail, along with corresponding simulations used to design and interpret the experiments. After that we report results from a first experimental test, including figures on its quantitative efficiency.

II. METHODS

A. Experiments

In order to conduct initial tests of *in situ* remoderation, minor modifications were made to the existing experimental configuration that has been described previously [8,9]. The set-up, shown in Fig. 1, was installed at the “open beam port” of the NEPOMUC beam line. There, positrons enter through a section for diagnosis of the beam intensity and shape [8,25]. A cylindrical “deflector” electrode in this section can be biased to a voltage sufficient to block the entire positron beam. Positrons that pass through the diagnostic section continue to be magnetically guided downward, between a pair of parallel rectangular electrodes. These generate the electric field that causes particles to undergo an $\mathbf{E} \times \mathbf{B}$ drift from the guiding field toward the closed field lines of the dipole trap. The permanent magnet (NdFeB, 0.6 T at the pole faces) and its trapping region are located below the $\mathbf{E} \times \mathbf{B}$ -drift zone.

A cylindrical wall of electrodes is installed at the outer radius of the trapping region, just inside the vacuum chamber boundary. The electrodes are divided into two vertically stacked sets, as a strategic tailoring of the electric fields around the magnet has been found helpful to achieve injection of slow positrons [9] (see also Fig. 2). A particularly important role in the injection process is played by the two wall electrodes toroidally located between the $\mathbf{E} \times \mathbf{B}$ plates (“Top1” and “Sector1” in Fig. 1).

Positrons that are successfully injected into the “confinement region” of the dipole trap—defined as the spatial region pervaded by magnetic field lines that intercept the magnet—“mirror” back and forth between the strong-field regions at the poles while toroidally drifting around the magnet. An illustration of the confinement region is provided in Fig. 3. After 180 degrees of toroidal drift, they can be intercepted by a square 10×10 mm steel plate (“target probe”). The radially insertable target probe is located on the side of the trap opposite from where injection occurs, and it can be retracted partially or fully out of the trapping volume. Relative measurements of the positron beam intensity on the target probe are routinely carried out by counting annihilation events using a collimated scintillation detector [10]. Additionally,

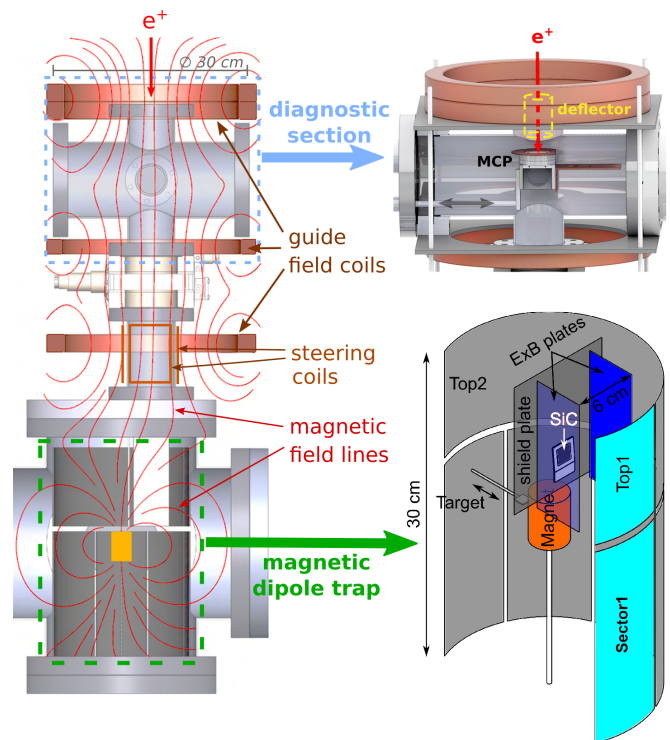


FIG. 1. A sketch (left) of our set-up for *in situ* remoderation and injection of positrons, along with more detailed views of the diagnostic section (top right) and magnetic dipole trap electrodes (bottom right). The NEPOMUC beam enters from above and can be characterized with a hollow cylindrical “deflector” electrode, a microchannel plate (MCP), and/or a metal plate with apertures. When the MCP/plate assembly is retracted (double arrow), the magnetically guided positrons continue down to the trapping experiment, where they enter between the $\mathbf{E} \times \mathbf{B}$ plates and are directed onto the SiC crystal, which is shown only in the bottom right panel. Bold, colored arrows are drawn as visual guides between different parts of the graphics.

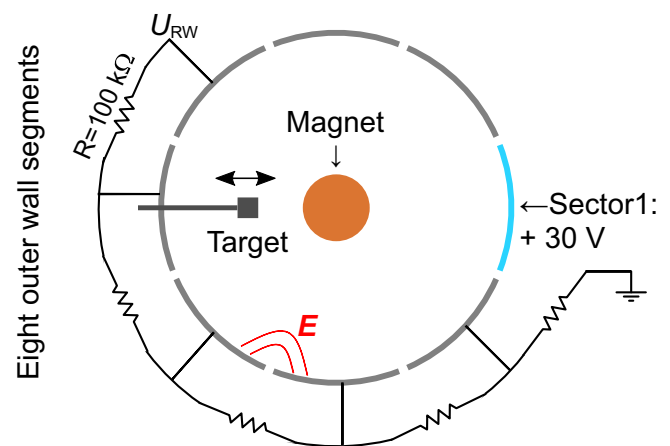


FIG. 2. Cut through the ring of electrodes in the equatorial plane of the magnetic field. An electric circuit used in part of our experiments to radially compress injected positrons is also shown. All resistors have the same nominal value. Ensuing electric field lines are sketched in one example location.

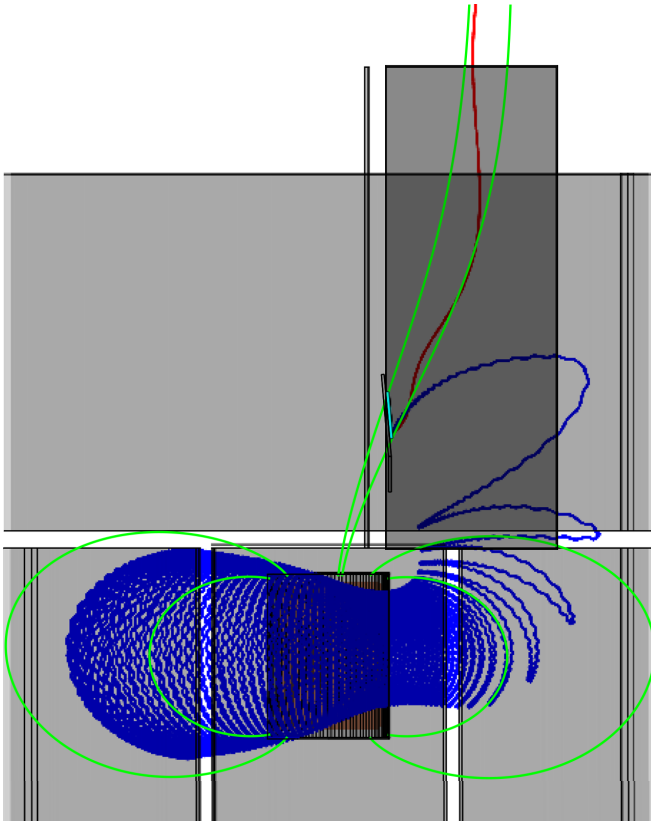


FIG. 3. Simulation of a single positron trajectory. The positron energy is 375 eV before remoderation (red part of the trajectory), and about 2 eV after remoderation (blue part). Selected magnetic field lines are plotted in green; these illustrate the angle of the magnetic field at the crystal (its cross section shown in cyan at the origin of the blue trajectory) and the middle and edge of the confinement region.

we measure the beam current using an amplifying current integrator built in-house [26]. These two measures of intensity are typically proportional to each other. (This suggests that secondary electrons and redistributed positrons produced by low-energy positrons incident on the probe tend not to be a significant factor for this measurement, due to a combination of the target surface properties and the magnetic and electrostatic geometries.) Additional wall sectors can be used to manipulate the radial distribution of the positrons as they toroidally drift around the magnet. This is done by applying static electric potentials with sequentially larger magnitudes in the drift direction of the positrons, producing electric fields with significant radial components [27]. These fields, combined with the \mathbf{B} field of the magnet, lead to an inward or outward $\mathbf{E} \times \mathbf{B}$ drift, depending on the polarity. A sketch of the arrangement is shown in Fig. 2. The spatial distribution of the positron cloud is measured by plotting the rate of positrons intercepting the target probe as a function of target probe insertion distance [8]. The fields sketched in Fig. 2 were only used where mentioned explicitly; in other experiments the wall electrodes apart from Sector1 and Top1 (Fig. 1) were kept at ground potential. For all experiments, the full set of electrode biases is given in the Supplemental Material (SM) [28].

For the *in situ* remoderation experiments described here, a holder for a reflection remoderator consisting of a silicon carbide (SiC)-plate was added to the set-up. This element was attached to the shield plate with an electrically insulated mount, enabling the application of a separate bias voltage; a photograph is shown in the SM [28]. The n-type 4H-SiC single-crystal of $15 \times 15 \times 0.25$ mm size was obtained commercially. The crystal was installed with an inclination angle of 5° to the vertical, resulting in an angle of 60 – 65° between the magnetic field direction and the crystal normal, as shown in Fig. 3. The magnetic field strength ranged from 13 mT at the top edge of the crystal to 22 mT at the bottom. Experiments were then typically conducted by firstly deciding on a bias voltage of the SiC remoderator (values of 0 V, 3 V, and 18 V were tried). Following that, optimal settings in the multidimensional parameter space influencing the positron injection process were found by monitoring counts on our scintillation detectors as a function of a two-dimensional parameter scan. In this way, in particular we optimized settings for the steering coils in the diagnostic section, voltages on the $\mathbf{E} \times \mathbf{B}$ plates and the “Top1” and “Sector1” segments of the rotating wall electrodes, and other elements as detailed below. (A pair of parameters was scanned at a time because of limitations in our experiment control software, but also practical consideration of the overall time spent for the optimization.)

The NEPOMUC primary beam was set to a nominal energy of 400 eV, for which we had previously measured the maximum positron flux at the NEPOMUC open beam port [29] (where the set-up described here is now installed). The size and shape of the primary beam were measured by the MCP detector in the diagnostic section. A slightly nonsymmetrical beam of 6.6×8.3 mm FWHM was obtained, in reasonable agreement with earlier experiments [25,26,30]; 80% of the intensity was found within a spot of approx. 14 mm in diameter, when measured in the guiding field of 5 mT. A representative MCP image is included in the SM [28].

B. Simulations

Preparation of the experiment had been guided by extensive simulations of positron trajectories. These initial simulations were carried out using SIMION [31] and assuming the use of a tungsten (W) remoderator. First, the trajectory of the incoming beam was calculated and used to decide where the remoderator crystal should be located. It was also verified that even with very large $\mathbf{E} \times \mathbf{B}$ biases, the positrons from the primary beam could not be drift injected onto trapped orbits in the confinement region (nor reach the target probe through other, chaotic orbits), due to their high energies and the modest magnetic field of the trap.

To establish that drift injection would be feasible for remoderated positrons reemitted from the crystal, an ensemble of particles was launched from an elliptical region on the remoderator, along the surface normal, with an energy of 2.9 eV, corresponding to the positron work function of W. A particle was considered injected when its trajectory resulted in precession around the dipole magnet, which was numerically judged by it exceeding a suitable lower temporal limit of the simulated propagation time. The inclination angle of the crystal was chosen such that drift injection into the trap was as

efficient as possible, with the constraint that only $\mathbf{E} \times \mathbf{B}$ plate biases were used. Favorable values for the remaining electrode voltages were determined subsequently, during which it was found that positively biasing the “Top1” and “Segment1” electrodes significantly increases injection efficiency, similar to our experiments with low-energy positron beams [9]. The choice for a fairly large angle between the magnetic field and crystal normal was thus a result of the optimization “path”; however, simulations performed after the experiments did not find this to have had any detrimental effect on the drift-injection process for the magnetic field strength and geometry of this trap.

Indeed, a wide variety of postexperiment simulations were conducted to facilitate comparison to and interpretation of the measured data; these were greatly helped by using the more efficient code AlGeoJ, which was developed in-house [32] and became available shortly after the experiments had been conducted. Extensions added to AlGeoJ made it possible to simulate the full beam path, including the remoderation step; these also incorporate the initial spatial distribution of the primary beam, as well as the voltages and steering coil currents that were actually applied in the experiment. (Remoderation is accounted for by an energy- and direction-changing step in the code; the details of positron scattering in the crystalline material are not part of the simulation.) A typical simulation of the trajectory of a remoderated and injected positron is shown in Fig. 3. The full set of electrode biases and another simulation are given in the SM [28].

III. RESULTS

A. Energy and spatial distribution of the primary positron beam

The parallel energy of the primary positron beam in the 5-mT guiding field was measured by scanning the bias voltage on the cylindrical deflector electrode at the entrance to our diagnostic section while recording annihilation counts on a target inside the diagnostic section. As shown in Fig. 4, the result was somewhat lower than the nominal setting, with the peak at ~ 350 eV, a half width at half maximum of ~ 15 eV on the high-energy side, and an extended low-energy tail with a half width at half maximum of ~ 55 eV. For similar settings of the primary beam, a perpendicular kinetic energy $\langle E_{\perp} \rangle$ of 18 eV was measured in an earlier experiment using a retarding field analyser [29]. We refer to this paper for a detailed discussion of the primary beam energy measurement.

A comparable—albeit higher-noise—version of the parallel energy measurement can be obtained by measuring annihilation counts directly on the target probe in the confinement region, again as a function of the upstream bias voltage blocking the positron beam. Note that “pure” drift injection of the high-energy primary beam into this trap is not feasible; the positrons detected in this measurement have undergone remoderation at the SiC crystal (blue trajectory in Fig. 3). Properties of the injected positrons are detailed in the next sections.

B. Kinetic energy of the injected positron beam

The energy of positrons that were successfully injected into the dipole field was determined by inserting the target probe

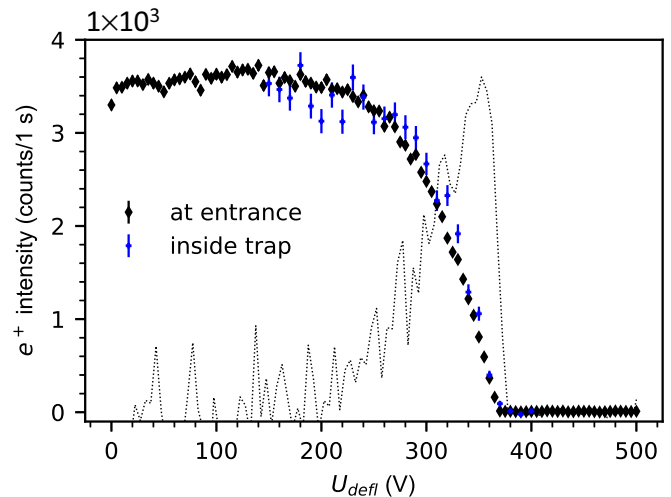


FIG. 4. Parallel energy of the primary positron beam in 5 mT. Black symbols show positron annihilation counts on the MCP target at the entrance of our experiment, as a function of the bias applied to the upstream “deflector” electrode U_{defl} . Blue symbols show the annihilation of remoderated, drift-injected positrons on the target probe in the confinement region, also as a function of “deflector” electrode bias, when the MCP target is retracted and the downstream experiment parameters (electrode biases and steering coil currents) have been suitably chosen. The blue curve has been arbitrarily scaled to match the black. Additionally, the numerical derivative of the “at entrance”-measurement is shown as a thin dotted line, on an arbitrary scale.

into the trapping region and measuring positron annihilation counts from the target probe as a function of the positive bias voltage U_{target} applied to it. Results of two such measurements are shown in Fig. 5, and a third is included in the SM [28]. As expected, there is a steep drop in annihilation counts (indicating that positrons do not have sufficient energy to reach the probe) when the target probe bias is set to more than a couple volts above the remoderator bias.

As described in the literature, 4H-SiC has a negative positron work function—i.e., positrons are ejected from the material with a few eV of kinetic energy—with reported values in the range of $-2.3(5)$ to $-2.7(1)$ eV [21,33]. However, a proper treatment of the prediction for the kinetic energy E_{kin}^+ of a positron emitted from the SiC crystal, as measured by the target probe, requires accounting not only for the biases applied to the two electrodes (for which we will use the shorthand U_S and U_t , with subscripts S and t for for “SiC” and “target”) but also the solid-state physics properties of the two materials. If no potentials are applied, the Fermi levels of the two electrodes are aligned. This leads to a shift of reference potentials for electron and positron states that can be expressed by the difference of the *electron* work functions $\phi_t^- - \phi_S^-$ [34]. Additionally, the positron work functions ϕ_t^+ of the SiC-crystal and the probe have to be taken into account. The full expression, including applied potentials, is given by [19]

$$E_{\text{kin}}^+ = eU_S - eU_t + \phi_t^- - \phi_S^- + \phi_t^+ - \phi_S^+. \quad (1)$$

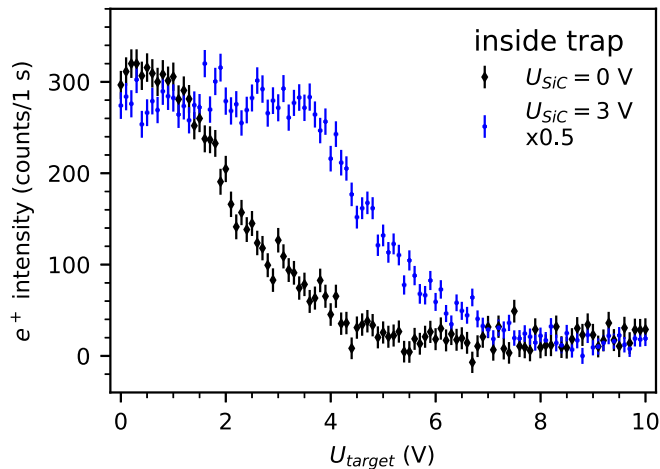


FIG. 5. Energy of the drift-injected positrons, measured for two different remoderator bias voltages: Black symbols show positron annihilation counts on the target probe in the confinement volume, as a function of the voltage applied to the target probe U_{target} , when the SiC remoderator was grounded. Blue symbols show the same measurement when the SiC remoderator was biased to +3 V, scaled down by a factor of two to ease comparison. (The higher count rate for the case with the positively biased remoderator has to do with the optimization of the drift injection process, which will be described in more detail later in the paper.) For each trace, the respective background signal (i.e., counts measured when the target probe was fully retracted) was subtracted.

We refer to the literature for the values of these quantities. For the stainless steel target, we use $\phi_t^- = 4.3$ eV [35], and as an approximation to its positron work function we take the value for polycrystalline Fe of $\phi_t^+ = -1.2$ eV [36]. The electron work function for 4H-SiC has been measured as $\phi_s^- = 4.50(8)$ to $4.75(8)$ eV, depending on the crystal structure at the surface [37]. We use $\phi_s^+ = -2.7(1)$ eV, although we note that lower values for the positron work function were measured for the epitaxially produced SiC surface [21] and in an older experiment [33], albeit with lower accuracy. Thus, the combined effect of the electron-related terms on the kinetic energy is between -0.45 and -0.2 eV, and together with the positron-related terms we have a correction to $eU_s - eU_t$ by $+1.05$ to $+1.3$ eV. A drop in the positron annihilation signal should therefore be observed at target bias voltages U_t that are this amount higher than the remoderator crystal bias U_s .

TABLE I. For three different values of the remoderator bias (top row), we list the target bias voltage U_{t0} above which annihilation counts on the target probe begin to decrease steeply (middle row), and the bias voltage at which the rate of descent is the steepest $U_{t\text{peak}}$. U_{t0} is defined as the largest value of the bias voltage at which counts are equal or higher than 90% of the count rate measured at $U_s = U_t$. U_{target} scans for cases with 0 V and 3 V applied to the SiC crystal were shown in Fig. 5.

SiC bias (V)	0.0	3.0	18.0
U_{t0} (V)	1.0	3.7	19.0
$U_{t\text{peak}}$ (V)	1.9(1)	4.7(2)	19.8(2)

Table I gives our measured values for the onset of steep signal drop (designated U_{t0} , see Table caption) in U_{target} scans, as well as the location of the peak in the derivative of these scans (designated $U_{t\text{peak}}$), for three different SiC biases. These are in very good agreement with the calculation described above; in particular, there is a constant (within the resolution of the measurements) offset, with a magnitude in the range of what was expected, between the SiC bias and those two key features of the U_{target} scans. As is evident from the difference between U_{t0} and $U_{t\text{peak}}$, as well as in the U_{target} scans themselves (Fig. 5), the drop-off in target probe annihilation with increasing U_{target} is relatively wide, with the peak in the derivative having a FWHM of 1.5 to 2 V. Apart from the underlying energy distribution we attribute these features to the complex geometry involved in our set-up, which includes the range of magnetic field strengths at the SiC crystal (13 to 22 mT), the even larger range of magnetic field strengths at the fully-inserted target probe (5 to 80 mT for probe positions between $r = 75$ and 25 mm, measured from the center of the magnet), and the wide spatial distribution and complexity of the positron trajectories. There is, nevertheless, no doubt that the annihilation signals on the target probe came from remoderated, drift-injected positrons.

The difference in intensity between the traces for the grounded and biased remoderator in Fig. 5 (note the scaling factor) is explained by an optimization of the upstream steering coils between the two measurements. The injection efficiency will be discussed in detail in a later section (Sec. III E).

In the simpler geometries of other experiments, the quantitative recording of the positron beam attenuation as a function of a variable potential barrier has been used as a method to determine the positron work function [34,36,38,39]. Different recipes on how to read these values from the measured data have been proposed [36,38] and a deliberate drop in the guiding magnetic field between remoderator and detector was engineered to increase precision [38]. Due to the complicating factors described in the previous paragraph, however, we abstain from attempting to constrain ϕ^+ from our measurements.

C. Role of the magnet bias

In earlier injection experiments with 5- and 20-eV positron beams from the NEPOMUC remoderator, we had found that the conditions for highest-efficiency injection required a positive bias voltage to be applied to the magnet case. In terms of the particle orbits, this bias “plugs the loss cone” via which particles can otherwise reach the magnet case; positrons with sufficiently small pitch angles relative to the magnetic field, such that they would not magnetically mirror before they hit the magnet case, are instead reflected by the electrostatic potential [9,10,40]. This remains true for the injection of *in situ*-remoderated positrons, with the optimal amount of magnet bias scaling with the SiC bias, as one would expect. Figure 6, for example, illustrates the influence of magnet bias on the injection of positrons from the grounded remoderator. The results in Fig. 5 used magnet biases of 0 V and 5 V for cases with remoderator bias of 0 V and 3 V, respectively. When the SiC crystal was biased to 18 V, a magnet bias of 20 V was found to be optimal. This is further evidence that

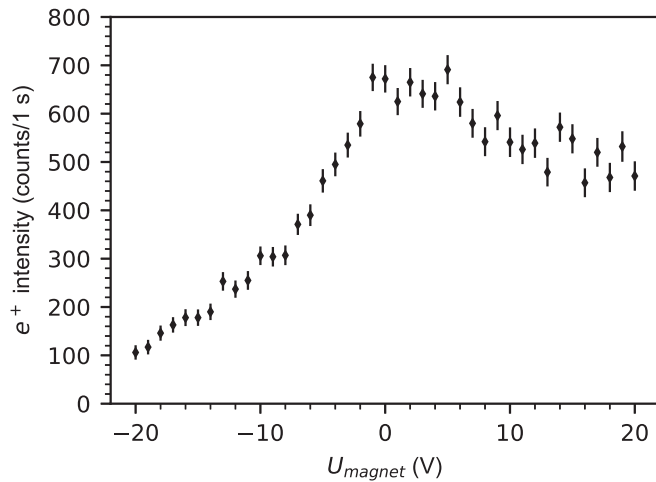


FIG. 6. The effect of magnet bias on injection of ~ 2 -eV, *in situ*-remoderated positrons: Annihilation counts from the target probe are plotted as a function of the bias voltage applied to the magnet case U_{magnet} . The SiC remoderator was grounded, and a background scan was subtracted.

the energy of the drift-injected positrons is determined by the bias applied to the remoderator.

D. Spatial profile of the injected positron cloud

As described previously, the spatial distribution of the injected positrons can be measured by recording how the current to the target probe and/or the annihilation counts coming from the target probe vary as a function of probe insertion. In general, the spatial profile depends on the settings of various electrodes that influence the injection process. Typical results for our combined remoderation-drift-injection approach are shown in Fig. 7. (These are for the case with the remoderator crystal grounded. Profiles for cases with the remoderator crystal biased were not substantially different; each case used an individually optimized set of electrode and steering coil settings.) The two measurement methods are compared in Fig. 7(a), and deliver identical profiles, within the experimental error. To quantitatively determine the width of the injected beam profile, we have analyzed an average of two consecutive measurements of the annihilation counts [Fig. 7(b)]. From a fit of an error function to the profile, we arrive at a position of the maximum at 54 mm and a width (FWHM) of 28 mm.

The wide spatial profile, combined with the large pitch angle of the remoderated positrons (which are reemitted approximately normal to the crystal and hence with a large angle relative to the magnetic field) raised the question as to whether a non-negligible fraction of positrons were drifting out to the wall during their toroidal transit, thereby being lost prior to detection with the target probe. To check for this possibility, we used the option of biasing the wall sectors to push positrons to smaller radii—the technique illustrated in Fig. 2. Figure 8 shows the results of these attempts, i.e., measurements of the spatial profile for different values of the potential drop $\Delta_{RW} = U_{RW}/5$ between each pair of segments. Positive as well as negative values of Δ_{RW} were tried, with the expectation that the latter would lead to an inward drift

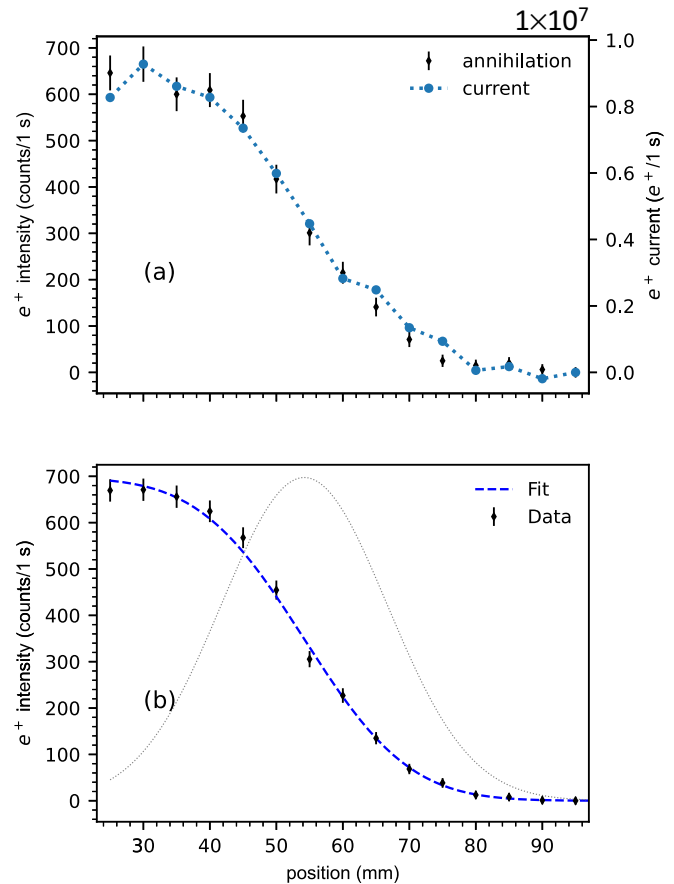


FIG. 7. Typical spatial profile of remoderated, injected positrons. (a) Annihilation counts from the target probe are plotted (left axis) as a function of the radial position of the probe, measured from the center of the magnet. A background has been subtracted. The positron rate recorded simultaneously with a current-integrating amplifier is shown for comparison (circles connected by a dotted line to guide the eye, right axis). (b) An error function (blue dashed line) has been fitted to the average of two measurements of the positron annihilation profile (black symbols); the underlying Gaussian profile (dotted line) is also shown, arbitrarily normalized.

of particles. This is qualitatively borne out by the results in Fig. 8. Indeed, a sharpening of the profile can also be seen for negative values of Δ_{RW} . That the maximum counts did not increase, however, shows that wall losses during the half-toroidal transit between drift injection and target probe detection were not appreciable. We have reported elsewhere in detail on methods to influence the positron orbits by DC and AC electric fields created by the sector electrodes [27,40].

E. Measured injection efficiencies

For the potential application of the methods tested here to the creation of an electron-positron plasma [7], as well as in positron experiments in general, the overall and individual efficiencies of the transport, remoderation, and drift injection of the beam are of high importance, due to the notorious scarcity of positrons even from bright sources such as NEPOMUC. An approximate accounting of what fraction of the positron beam survives through each step of the process, obtained by

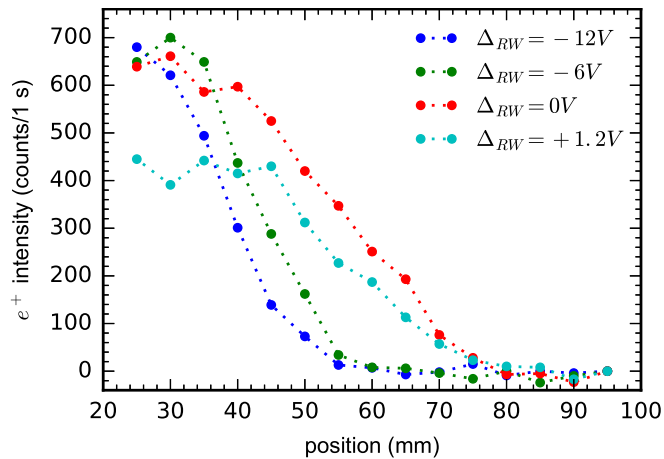


FIG. 8. Manipulation of the spatial profile using wall sector biases: Positron annihilation counts on the target probe are plotted vs the probe position, for different values of a DC voltage difference between subsequent wall segments outside the confinement region, in the direction of the positrons’ toroidal drift (Fig. 1). A background has been subtracted.

combining measurements (made with the current-integrating amplifier during the experiment campaign) with follow-up simulations, is summarized in Table II.

The NEPOMUC diagnostic “beam monitor 2” is located relatively close to the source; the positron rate measured there was only $\sim 4 \times 10^8 e^+/s$, about 75% of what had previously been measured tens of meters downstream at the open beam port [29]. This time, measurements at the open beam port initially corresponded to a positron rate of $\sim 2.7 \times 10^8 e^+/s$; over the course of the four-day experiment campaign, this decreased to $\sim 1.7 \times 10^8 e^+/s$ without clear reason. Additionally, toward the end of the campaign it became clear that we also needed to take into account the non-negligible contribution from secondary electrons produced by 400-eV positrons; by measuring the beam current and counts as a function of scans of the bias applied to the deflector electrode (see Fig. 1), we determined the true incoming rate of positrons at our diagnostic set-up to be $1.3 \times 10^8 e^+/s$. Thus, the largest positron “leak” in the process came from beam guiding losses, before the positrons even reached the open beam port; this is

TABLE II. Positron rates measured during the experiment campaign, supplemented with simulation data (*), provide a rough picture of where positrons were lost during the transport, remoderation, and drift injection processes. Overall the emission efficiency amounted to up to $\sim 15\%$. Further details are given in the text and in Table III.

Location	e^+ rate ($10^7/s$)
beam monitor 2	39 ± 4
open beam port (apparent)	20 ± 5
open beam port (actual)	13.3 ± 0.4
incident on SiC (*)	11
reemitted from SiC (*)	4
target probe	1-2

TABLE III. The maximum rate of positrons detected at the target probe is given for three different remoderator biases.

SiC bias (V)	0	2.5	18
e^+ rate ($10^7/s$)	0.9	0.8	2.0

because the beam line was not designed to transport a beam at kinetic energies of several hundred eV, nor a beam with the wider spatial spread of the primary beam.

Out of the $1.3 \times 10^8 e^+/s$ that arrived at the open beam port, up to $2.0 \times 10^7 e^+/s$ were successfully transported to the target probe via the combined remoderation-drift scheme, for an efficiency of $15(\pm 1)\%$. (This was achieved with the remoderator biased to 18 V; for the cases with lower remoderator bias, less than about half that rate could be achieved, as indicated in Table III. Possible reasons for this, as determined from follow-up simulations, will be discussed shortly.) For comparison, $2.3 \times 10^7 e^+/s$ were injected with our original lossless drift injection method [13]; in that scheme, we are limited by the efficiency for the NEPOMUC remoderator (e.g., 2.6% in [30]). Thus, our scheme actually performed remarkably well, despite being lossy, and by understanding and reducing or eliminating the loss mechanisms, it has the potential for significant improvement.

F. Follow-up simulations

After the experiment campaign, extensive simulations were conducted in order to disentangle the overall maximum $15(\pm 1)\%$ efficiency at our set-up into the individual efficiencies of the different steps of our new combined injection scheme (steering of the beam onto the SiC remoderator, remoderation, and drift injection), to better understand why the efficiency was highest for the case with the remoderator biased to 18 V, and to identify ways to improve the set-up in future applications.

To simulate the spatial distribution of the incoming primary beam, starting points of the simulated trajectories were randomly generated based on the MCP image of the positron beam shown in Fig. S2 within SM [28]. The center of this starting distribution within the beam line could be scanned in the horizontal plane; these two free parameters are a stand-in for the influence of undetermined stray fields, possible imperfect alignment of coils, and similar uncertain deviations from the nominal arrangement. Typically 1000 positrons per simulation setting were launched with parallel and perpendicular velocity spreads akin to the measured values, with the resulting full-orbit trajectories under the influence of the 3D electric and magnetic fields followed until they intercepted with material surfaces. Positrons that impinged on the SiC crystal were re-launched in the direction of the crystal normal with an energy of 2.1 eV. Details of the simulation configuration were primarily taken from the experimental settings, but they could also be varied to explore which aspects are necessary to yield agreement to the measurements, the sensitivity of that agreement, and the physical mechanisms at play.

It was found that 85–90% of the incoming positrons can be expected to hit the remoderator crystal (rather than the surrounding holder), and this is fairly insensitive to parameter

variations. However, whether or not a remoderated positron is successfully drift-injected is very sensitively dependent on the horizontal coordinate of its launch position on the crystal. (As mentioned, the launch position of a simulated, remoderated positron from the crystal was assumed identical to the point of impact of the respective primary positron.) This means that the effective “target” for beam steering is not the entire crystal but rather a 1.5- to 2-mm wide vertical strip on it. (Positrons launched too far to one side of this strip quickly return to the remoderator crystal, having been electrostatically reflected by the potential of the positively biased $\mathbf{E} \times \mathbf{B}$ plate; positrons launched too far to the other side of this strip gain enough kinetic energy from their proximity to the negatively biased $\mathbf{E} \times \mathbf{B}$ plate that they escape upward out of the trap before they can be drift injected into the confinement region.) A reduced fraction of the incident beam can hit this narrower target range, no matter how well optimized the beam guiding might be; this results in a maximum efficiency of $\sim 45\%$ for the drift injection step of the process, for the experimental settings used in the 18-V remoderator bias case. (We also would like to note that in our simulations the remoderator crystal is assumed to behave as a conductor, while in fact it is a semiconductor. In how far the actual potential distribution on the crystal surface is influenced by its solid-state properties was outside the scope of our investigation.)

For the experimental settings used in the 3-V remoderator bias case, the maximum efficiency of the drift injection step was $\sim 39\%$ —i.e., only slightly lower. However, the optimal steering settings in the simulation deviated slightly from those used in the experiment. This leads us to tentatively conclude that the lower rates of positrons measured at the target probe in the cases with the lower remoderator bias are not a fundamental problem with the drift-injection step of the resulting lower-energy positrons; rather, they seem to be due to the experimental parameter optimization having not been fully successful, due to the aforementioned narrow optimum.

G. Remoderation efficiency

Combining the overall measured maximum efficiency of $15(\pm 1)\%$ (from Sec. III E) with the efficiencies estimated from the follow-up simulations (from Sec. III F) allows us to calculate an estimate for the remoderation efficiency, which comes out to 36–41%. While lower than efficiencies found in the literature for 4H-SiC, this might not be unexpected, given that our incoming positrons are not only lower in energy but also incident on the crystal at a steep angle.

This estimate can also be compared to another type of measurement conducted during the experiment campaign, in which counts from a second scintillator detector with a collimated view of the region around the remoderator crystal were recorded while the bias on the remoderator was scanned. All other electrodes, including the $\mathbf{E} \times \mathbf{B}$ plates, were grounded. A typical result is plotted in Fig. 9.

We expect that for a negative bias voltage with a magnitude exceeding the work function, all positrons—even remoderated ones—annihilate in the crystal. If instead the bias voltage is tuned towards positive values, the remoderated positrons can escape from the crystal, annihilating outside

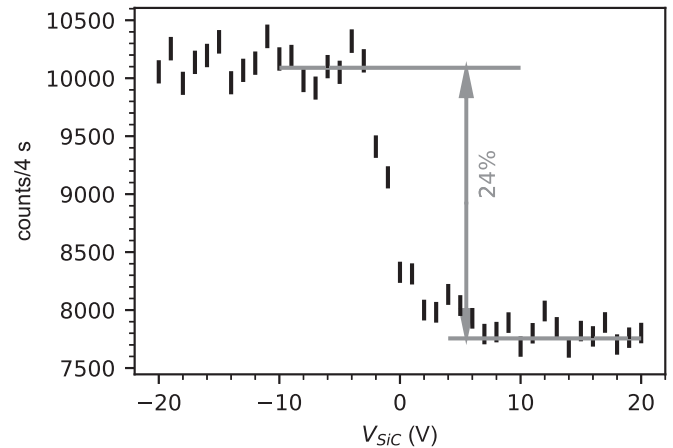


FIG. 9. Annihilation counts from the region of the remoderation crystal as a function of crystal bias voltage. Remoderated positrons can escape the crystal—and thus avoid annihilation—as soon as this voltage becomes positive. Therefore the relative decrease of signal indicated graphically is related to—but not identical to—the remoderation efficiency.

of the viewing window of the detector, and the signal drops. An average of several repeats of this measurement resulted in a bias-induced drop in annihilation counts of 24(1)%. This figure cannot be directly identified with the remoderation efficiency ε , however, because the crystal holder is also within the field of view of the detector; therefore, positrons hitting the holder will contribute to the annihilation signal, as well. The size of the step therefore underestimates the remoderation efficiency.

Simulations run with the parameters of the measurements shown in Fig. 9 found that the measured signal drop is in rough agreement with an $\varepsilon = 0.3$ but depends on the choice of free parameters (which affect what fraction of the primary beam is incident on the SiC, versus the holder).

H. Possible improvements and future applications

Simulations were also used to explore how hypothetical adaptations to the experiment set-up might affect the efficiency of *in situ* moderation. For example, tilting the crystal back to be less oblique to the magnetic field was not found to have a large effect on the trajectories of the remoderated positrons emitted from its surface; the narrow horizontal “sweet spot” on the SiC that the incoming primary beam needs to target, in order for the remoderated positrons to be drift injected as efficiently as possible, was essentially unaffected. On the other hand, the addition of a new electrode at the top of the chamber, just below the lid, showed great promise for increasing the range of horizontal locations on the crystal from which remoderated positrons can be drift-injected; this in turn would significantly increase the achievable efficiency of that step in the process.

However, future pair plasma experiments will not be using the NEPOMUC primary beam as an input to the toroidal traps, nor will they be done in the prototype trap used for the proof-of-concept experiments we described here. Instead, they will receive pulses of positrons that will be accumulated and stored in linear traps, and these will in turn be injected into

higher-field traps with their own unique magnetic geometries. Therefore, future experimental applications of our new *in situ* moderation scheme will require design/specification/scoping simulations that incorporate these new conditions.

IV. SUMMARY

We have demonstrated a spatially compact scheme for injection of positrons from a reactor-based positron source into a trapping magnetic field. The largest losses occurred in the beam line on the way to the experiment, due to the inherent challenges involved in guiding the wider, higher-energy primary beam through a beam line not designed for it. Positrons that reached the experiment could be injected with an efficiency of up to $15(\pm 1)\%$, and simulations indicate the loss mechanisms and how these could be ameliorated in future implementations.

Although our first demonstration of an *in situ* moderation scheme did not immediately result in a higher rate positrons injected into our current prototype trap (where the modest magnetic field strength of the confinement allows us to successfully drift inject a wide range of energy distributions), it is

an important proof-of-principle demonstration of a technique that may be the key to getting positrons into the higher-field traps we plan to use for pair plasma confinement. In particular, by placing a positron remoderator near to the trapping region we add another degree of freedom to the design space for future injection schemes.

The data that support the findings of this study are available upon reasonable request from the authors.

ACKNOWLEDGMENTS

The authors acknowledge contributions of Sebastian Voburger to setting up the experiment. E.V.S. gratefully acknowledges funding from the Helmholtz Association. This work was partially funded by the Deutsche Forschungsgemeinschaft via Grants Hu 978/15-1 and Sa 2788/2-1 and has received funding from the European Research Council (ERC) under the European Union's Horizon 2020 research and innovation programme under Grant Agreement No. 741322. This work is based upon experiments performed at the NEPOMUC positron beam facility operated by FRM II at the Heinz Maier-Leibnitz Zentrum (MLZ), Garching, Germany.

-
- [1] K. Blaum, Y. N. Novikov, and G. Werth, Penning traps as a versatile tool for precise experiments in fundamental physics, *Contemp. Phys.* **51**, 149 (2010).
- [2] M. G. Kozlov, M. S. Safronova, J. R. Crespo López-Urrutia, and P. O. Schmidt, Highly charged ions: Optical clocks and applications in fundamental physics, *Rev. Mod. Phys.* **90**, 045005 (2018).
- [3] M. Ahmadi, B. X. R. Alves, C. J. Baker, W. Bertsche, E. Butler, A. Capra, C. Carruth, C. L. Cesar, M. Charlton, S. Cohen *et al.*, Antihydrogen accumulation for fundamental symmetry tests, *Nat. Commun.* **8**, 681 (2017).
- [4] D. W. Fitzakerley, M. C. George, E. A. Hessels, T. D. G. Skinner, C. H. Storry, M. Weel, G. Gabrielse, C. D. Hamley, N. Jones, K. Marable *et al.*, Electron-cooled accumulation of 4×10^9 positrons for production and storage of antihydrogen atoms, *J. Phys. B: At. Mol. Opt. Phys.* **49**, 064001 (2016).
- [5] A. J. H. Donné, The European roadmap towards fusion electricity, *Phil. Trans. R. Soc. A: Math. Phys. Eng. Sci.* **377**, 20170432 (2019).
- [6] V. Tsytovich and C. B. Wharton, Laboratory electron-positron plasma—A new research object, *Comments Plasma Phys. Cont. Fusion* **4**, 91 (1978).
- [7] M. R. Stoneking, T. S. Pedersen, P. Helander, H. Chen, U. Hergenhahn, E. V. Stenson, G. Fiksel, J. von der Linden, H. Saitoh, C. M. Surko *et al.*, A new frontier in laboratory physics: Magnetized electron–positron plasmas, *J. Plasma Phys.* **86**, 155860601 (2020).
- [8] H. Saitoh, J. Stanja, E. V. Stenson, U. Hergenhahn, H. Niemann, T. S. Pedersen, M. R. Stoneking, C. Piochacz, and C. Hugenschmidt, Efficient injection of an intense positron beam into a dipole magnetic field, *New J. Phys.* **17**, 103038 (2015).
- [9] E. V. Stenson, S. Nißl, U. Hergenhahn, J. Horn-Stanja, M. Singer, H. Saitoh, T. S. Pedersen, J. R. Danielson, M. R. Stoneking, M. Dickmann, and C. Hugenschmidt, Lossless Positron Injection into a Magnetic Dipole Trap, *Phys. Rev. Lett.* **121**, 235005 (2018).
- [10] J. Horn-Stanja, S. Nißl, U. Hergenhahn, T. S. Pedersen, H. Saitoh, E. V. Stenson, M. Dickmann, C. Hugenschmidt, M. Singer, M. R. Stoneking, and J. R. Danielson, Confinement of Positrons Exceeding 1 s in a Supported Magnetic Dipole Trap, *Phys. Rev. Lett.* **121**, 235003 (2018).
- [11] T. G. Northrop and E. Teller, Stability of the adiabatic motion of charged particles in the earth's field, *Phys. Rev.* **117**, 215 (1960).
- [12] T. S. Pedersen, J. R. Danielson, C. Hugenschmidt, G. Marx, X. Sarasola, F. Schauer, L. Schweikhard, C. M. Surko, and E. Winkler, Plans for the creation and studies of electron-positron plasmas in a stellarator, *New J. Phys.* **14**, 035010 (2012).
- [13] E. V. Stenson, J. Horn-Stanja, M. R. Stoneking, and T. S. Pedersen, Debye length and plasma skin depth: Two length scales of interest in the creation and diagnosis of laboratory pair plasmas, *J. Plasma Phys.* **83**, 595830106 (2017).
- [14] D. B. Cassidy, T. H. Hisakado, H. W. K. Tom, and A. P. Mills, Efficient production of Rydberg positronium, *Eur. Phys. J. D* **72**, 53 (2018).
- [15] J. R. Danielson, D. H. E. Dubin, R. G. Greaves, and C. M. Surko, Plasma and trap-based techniques for science with positrons, *Rev. Mod. Phys.* **87**, 247 (2015).
- [16] M. Singer, S. König, M. R. Stoneking, P. Steinbrunner, J. R. Danielson, L. Schweikhard, and T. S. Pedersen, Non-neutral plasma manipulation techniques in development of a high-capacity positron trap, *Rev. Sci. Instrum.* **92**, 123504 (2021).
- [17] N. Oshima, T. M. Kojima, M. Niigaki, A. Mohri, K. Komaki, and Y. Yamazaki, New Scheme for Positron Accumulation in Ultrahigh Vacuum, *Phys. Rev. Lett.* **93**, 195001 (2004).

- [18] C. J. Baker, W. Bertsche, A. Capra, C. L. Cesar, M. Charlton, A. Cridland Mathad, S. Eriksson, A. Evans, N. Evetts, S. Fabbri *et al.*, Sympathetic cooling of positrons to cryogenic temperatures for antihydrogen production, *Nat. Commun.* **12**, 6139 (2021).
- [19] C. Hugenschmidt, Positrons in surface physics, *Surf. Sci. Rep.* **71**, 547 (2016).
- [20] R. Suzuki, T. Ohdaira, A. Uedono, Y. K. Cho, S. Yoshida, Y. Ishida, T. Ohshima, H. Itoh, M. Chiwaki, T. Mikado, T. Yamazaki, and S. Tanigawa, Investigation of positron moderator materials for electron-linac-based slow positron beamlines, *Jpn. J. Appl. Phys.* **37**, 4636 (1998).
- [21] A. M. M. Leite, P. Debu, P. Pérez, J.-M. Reymond, Y. Sacquin, B. Vallage, and L. Liskay, Efficient positron moderation with a commercial 4H-SiC epitaxial layer, *J. Phys.: Conf. Ser.* **791**, 012005 (2017).
- [22] C. Hugenschmidt, C. Piochacz, M. Reiner, and K. Schreckenbach, The NEPOMUC upgrade and advanced positron beam experiments, *New J. Phys.* **14**, 055027 (2012).
- [23] C. Piochacz, E. Erdnöß, T. Gigl, N. Grill, and C. Hugenschmidt, Enhancement and transformation of the phase space density of the NEPOMUC positron beam, *J. Phys.: Conf. Ser.* **505**, 012027 (2014).
- [24] M. Dickmann, W. Egger, G. Kögel, S. Vohburger, and C. Hugenschmidt, Upgrade of the nepomuc remoderator, *Acta Phys. Pol. A* **137**, 149 (2020).
- [25] J. Horn-Stanja, E. V. Stenson, M. R. Stoneking, M. Singer, U. Hergenbahn, S. Nißl, H. Saitoh, T. S. Pedersen, M. Dickmann, C. Hugenschmidt, and J. R. Danielson, Injection of intense low-energy reactor-based positron beams into a supported magnetic dipole trap, *Plasma Res. Express* **2**, 015006 (2020).
- [26] U. Hergenbahn, J. Horn-Stanja, S. Nissl, T. S. Pedersen, H. Saitoh, E. V. Stenson, M. R. Stoneking, M. Dickmann, C. Hugenschmidt, M. Singer *et al.*, Progress of the apex experiment for creation of an electron-positron pair plasma, *AIP Conf. Proc.* **1928**, 020004 (2018).
- [27] H. Saitoh, J. Horn-Stanja, S. Nißl, E. V. Stenson, U. Hergenbahn, T. S. Pedersen, M. Singer, M. Dickmann, C. Hugenschmidt, M. R. Stoneking *et al.*, Manipulation of positron orbits in a dipole magnetic field with fluctuating electric fields, *AIP Conf. Proc.* **1928**, 020013 (2018).
- [28] See Supplemental Material at <http://link.aps.org/supplemental/10.1103/PhysRevResearch.5.023172> for additional details of the experiments, including a photograph of the SiC crystal mount, complete electrode bias settings, as well as a complementary, simulated single-particle trajectory.
- [29] J. Stanja, U. Hergenbahn, H. Niemann, N. Paschkowski, T. S. Pedersen, H. Saitoh, E. V. Stenson, M. R. Stoneking, C. Hugenschmidt, and C. Piochacz, Characterization of the NEPOMUC primary and remoderated positron beams at different energies, *Nucl. Instrum. Methods Phys. Res., Sect. A* **827**, 52 (2016).
- [30] C. Hugenschmidt, H. Ceeh, T. Gigl, F. Lippert, C. Piochacz, M. Reiner, K. Schreckenbach, S. Vohburger, J. Weber, and S. Zimmik, Positron beam characteristics at NEPOMUC upgrade, *J. Phys.: Conf. Ser.* **505**, 012029 (2014).
- [31] D. A. Dahl, SIMION for the personal computer in reflection, *Int. J. Mass Spectrom.* **200**, 3 (2000).
- [32] S. Nißl, Numerical investigations into injection and confinement of single particles in a magnetic dipole trap, Master's thesis, Technische Universität München, 2018.
- [33] C. C. Ling, H. M. Weng, C. D. Beling, and S. Fung, Experimental investigation of slow-positron emission from 4h-SiC and 6h-SiC surfaces, *J. Phys.: Condens. Matter* **14**, 6373 (2002).
- [34] C. A. Murray, A. P. Mills, and J. E. Rowe, Correlations between electron and positron workfunctions on copper surfaces, *Surf. Sci.* **100**, 647 (1980).
- [35] R. G. Wilson, Vacuum thermionic work functions of polycrystalline Be, Ti, Cr, Fe, Ni, Cu, Pt, and type 304 stainless steel, *J. Appl. Phys.* **37**, 2261 (1966).
- [36] M. Jibaly, A. Weiss, A. R. Koymen, D. Mehl, L. Stiborek, and C. Lei, Measurement of the positron work functions of polycrystalline Fe, Mo, Ni, Pt, Ti, and V, *Phys. Rev. B* **44**, 12166 (1991).
- [37] M. Wiets, M. Weinelt, and T. Fauster, Electronic structure of SiC(0001) surfaces studied by two-photon photoemission, *Phys. Rev. B* **68**, 125321 (2003).
- [38] A. Nangia, J. H. Kim, A. H. Weiss, and G. Brauer, Experimental determination of positron-related surface characteristics of 6H-SiC, *J. Appl. Phys.* **91**, 2818 (2002).
- [39] C. Hugenschmidt, B. Straßer, and K. Schreckenbach, Investigation of positron work function and moderation efficiency of Ni, Ta, Pt and W(1 0 0), *Appl. Surf. Sci.* **194**, 283 (2002).
- [40] S. Nißl, E. V. Stenson, U. Hergenbahn, J. Horn-Stanja, T. S. Pedersen, H. Saitoh, C. Hugenschmidt, M. Singer, M. R. Stoneking, and J. R. Danielson, Positron orbit effects during injection and confinement in a magnetic dipole trap, *Phys. Plasmas* **27**, 052107 (2020).